Pinch-off Dynamics and Extensional Relaxation Times of Intrinsically Semi-Dilute Polymer Solutions Characterized by Dripping-onto-Substrate Rheometry

Jelena Dinic, Madeleine Biagioli, Vivek Sharma

Department of Chemical Engineering, University of Illinois at Chicago, Illinois 60607
Correspondence to: V. Sharma (E-mail:viveks@uic.edu)

Received 19 April 2017; accepted 24 May 2017; published online 26 June 2017
DOI: 10.1002/polb.24388

ABSTRACT: Stream-wise velocity-gradients associated with extensional flows arise in thinning liquid necks spontaneously formed during jetting, printing, coating, spraying, atomization, and microfluidic-based drop formation. In this contribution, we employ Dripping-onto-Substrate (DoS) rheometry protocols to measure the extensional rheology response of intrinsically semi-dilute polymer solutions by visualizing and analyzing capillary-driven thinning of a columnar neck formed between a nozzle and a sessile drop. We show that extensional viscosity that quantifies the resistance to stream-wise velocity gradients is orders of magnitude higher than the shear viscosity. Although shear flows only weakly perturb the chain dimensions, extensional flows can strongly stretch and orient the chains, thus influencing both intra- and inter-chain interactions. We find that the extensional relaxation times for intrinsically semi-dilute PEO solutions in a good solvent for five different molecular weights increase linearly with concentration, exhibiting a stronger concentration dependence than observed for dilute solutions, or anticipated by blob models, developed for relaxation of weakly perturbed chains in a good solvent. The observed distinction between the concentration-dependent relaxation dynamics of intrinsically dilute and semi-dilute solutions arises due the complex influence of stretching, conformational anisotropy, and polymer concentration on excluded volume and hydrodynamic interactions of flexible, highly extensible polymers. © 2017 Wiley Periodicals, Inc. J. Polym. Sci., Part B: Polym. Phys. **2017**, *55*, 1692–1704

KEYWORDS: capillarity; DoS rheometry; extensional rheology; printability; semi-dilute polymer solutions

INTRODUCTION Drop formation and liquid transfer in jetting,[1–11] printing,[11–16] coating, and spraying[17] as well as microfluidic drop/particle formation[18] applications are accompanied by formation of unstable columnar liquid necks that undergo surface tension driven thinning and pinch-off. Advances in high-speed imaging and visualization methods, coupled with advances in theory and simulation methods for free surface flows,[6–23] have resulted in a fairly comprehensive characterization and understanding of capillary-thinning dynamics for simple, Newtonian fluids. For Newtonian fluids, the complex interplay of inertial, viscous and capillary stresses before and after breakup leads to neck thinning dynamics that can often be described by universal scaling laws, and self-similar neck evolution manifested in experiments.[6–16,20–27] Stream-wise velocity-gradients associated with extensional flows arise in thinning liquid necks spontaneously formed during printing,[6–16,28–34] spraying and atomization[17,35–39] and fiber spinning.[40–45] Although extensional viscosity (η_E) that quantifies the resistance to extensional flows is only three times the shear viscosity for Newtonian fluids as was pointed out by Trouton,[46] the extensional viscosity for polymer solutions can be orders of magnitude higher (10^4–10^6 reported for dilute polymer solutions).[10–13,47–50] A particular challenge for describing pinch-off dynamics of polymer solutions is the need for quantifying the non-Newtonian extensional rheology response.

It is well-established that in comparison with Newtonian fluids of the same viscosity and surface tension, additional viscoelastic stresses contributed by the presence of polymers result in a measurable delay in pinch-off that can be used for obtaining a measure of both extensional viscosity (transient $\eta_E^t = \eta_E(\dot{\varepsilon}, \varepsilon, t)$ as well as steady terminal extensional viscosity, η_E^∞)[6–17,28–64] and an extensional relaxation time, λ_E that correlates with the characteristic time needed for chain relaxation after an extensional or stretching deformation.[11,54,65–67] Strain-rate dependent extensional viscosity of polymer solutions can be measured using stagnation point flows realized in four roll mills,[68] cross-slot rheometers,[50,69,70] and opposed jet extensional rheometers,[71,72] as extensional rate can be controlled independently, and either resulting pressure drop, or birefringence, can be measured. In contrast, the intrinsic balance of stresses sets the extensional rates realized in capillary-driven thinning experiments.

Furthermore, as the transient extensional viscosity measured in most techniques often depends on strain, strain rate and the entire deformation history of the fluid,[11,43,47,73] capillary-thinning based measurements are more significant for determining printability, jettability or sprayability as the strains, strain rate and deformation history mimic the values realized in the realistic capillary-driven flows. Exceptionally high extensional strain rates ($\dot{\varepsilon} > 10^3\ s^{-1}$) are hard to reach or obtain in macroscopic or microfluidic stagnation-flow based measurements of viscoelastic, low viscosity fluids due to limitations of experimental techniques (see discussion in Sharma et al.[10]), or due to inertial effects, or the onset of elastic instabilities (observed for $\lambda\dot{\varepsilon} \gg 1$).[50,74–78] However, relatively high extension rates ($\dot{\varepsilon} > 10^3\ s^{-1}$) can be realized in capillary-thinning experiments,[10] allowing measurements of elastic effects even for weakly viscoelastic fluids,[10,12] and in many cases, the steady terminal extensional viscosity values can also be measured.[10,48,49,65] Though capillary thinning dynamics have been used extensively for analyzing the extensional rheology response of dilute polymer solutions,[10–12,28,29,48,49,54,79–81] relatively few studies have explored the response of intrinsically semi-dilute polymer solutions systematically.[82,83] The present contribution is motivated by the need for a deeper understanding of the capillary-driven thinning and pinch-off dynamics, transient extensional viscosity, concentration-dependent relaxation time, and consequently printability of unentangled, semi-dilute solutions.

Polymer solutions are considered dilute below a critical overlap concentration, $c^* \approx M_w/N_A R_g^3$ calculated by equating the volume per coil to the size of unperturbed chain at equilibrium.[84] Here, N_A is Avogadro's number and the radius of gyration or chain size $R_g \propto M_w^{\nu}$ depends on molecular weight, M_w and excluded volume (EV) interactions. Solvent quality determines the values of EV exponent: $\nu = 0.5$ for θ-solvent (ideal chains) to $\nu = 0.588$ for good solvent (expanded coils). By definition, as static and dynamic properties of dilute solutions are not influenced by interchain interactions, the dynamics are typically described using single chain models by accounting for chain flexibility, entropic resistance to stretching, solvent-mediated hydrodynamic interactions and EV interactions.[66,84–86] For dilute solutions, the macromolecular dynamics in quiescent conditions (dynamic light scattering) or in shear flow for dilute solutions are captured quite well by Zimm model,[84–87] a single chain model that accounts for both EV and hydrodynamic interactions. In contrast, the original Rouse model[84,85,88] that neglects both effects (and is inconsistent with the measured response of dilute solutions) is found to describe the dynamics of unentangled melts quite well.

Unperturbed polymer coils in solution interpenetrate for intrinsically semi-dilute solutions with concentrations $c > c^*$, and the macromolecular dynamics in such semi-dilute polymer solutions[85,86] even under shear flow are relatively challenging to understand and describe due to the influence of large concentration fluctuations as well as local concentration-dependent hydrodynamic and EV interactions. In this article, we focus on intrinsically semi-dilute, unentangled polymer solutions ($1 < c/c^* < c_e/c^*$), such that the upper limit to the concentrations investigated is set by entanglement concentration, c_e, beyond which topological interactions play a role. We experimentally probe the dynamics of stretched chains in solutions with polymer concentration above their overlap concentration ($c/c^* > 1$). Since a strong overlap exists between macromolecules even in their quiescent state, we refer to these as intrinsically semi-dilute solutions. In this study, we contrast their behavior against solutions with $c/c^* < 1$ that are considered dilute under quiescent conditions or in shear, but referred to as effectively semi-dilute in many extensional rheology studies, due to increase degree of overlap and interchain interactions in stretched chains.

The progressive screening of both EV and hydrodynamic interactions in intrinsically semi-dilute solutions can be captured to a good approximation by using composite Rouse-Zimm model or the blob models.[86,89] In the blob models, EV and/or hydrodynamic interactions play a role below a length scale shorter than the blob size ξ. On length scales larger than the blob size, $r > \xi$ Rouse-like dynamics apply due to screening of hydrodynamic as well as EV interactions by the presence of overlapping chains. Although shear flows only weakly perturb the chain dimensions, extensional flows can stretch and even break the chains.[9,69,90] Strong extensional flows can lead to coil-stretch transition,[84,91,92] and accumulated strain could lead to extension of chains to their full, finite extensibility. The intrachain and interchain interactions dramatically change as the chain gets progressively stretched by extensional flow, impacting both the magnitude and the concentration-dependent scaling of extensional viscosity and relaxation time.[12,54,66,79,80] Even the solutions considered dilute based on their equilibrium coil size, due to stretching in extensional flow develop a fair degree of overlap, and several authors contrast their behavior with semi-dilute solutions.[12,48,49,54,79,90] But, the extensional relaxation time measured for such solutions increases with concentration $\lambda_E \propto c^m$ with the exponent displaying values $0.31 < m < 1$ that are distinct from $m = 0.31$ expected for good solvents and $m = 1$ for theta solvents. Furthermore, both coil-coil overlap and EV interactions are influenced by the degree of stretching, conformational anisotropy, and tension applied to the chains, and standard blob theory was not designed for accounting of all the three effects.

In the 1970s, de Gennes and Pincus postulated that the single polymer chains under tension can be described by considering an equivalent chain made up of tension blobs[89,93,94] (Or Pincus blobs) of size ξ_t, such that structural anisotropy and the influence of the applied tension on intrachain interactions play a role only above ξ_t. At the molecular level, the question that remains unanswered is how such chain of Pincus blobs relaxes or behaves when surrounded by a sea of similarly stretched chains in a good solvent. Prabhakar and coworkers[66,67] outlined related theoretical challenges and open questions quite recently for unentangled polymer solutions in a theta solvent.[66,67] Their new constitutive model probes the influence of stretching on polymer dynamics by combining the blob picture with an

assessment of conformation-dependent drag, and infers that stretching causes intermolecular interactions to become stronger in the dilute regime and weaker in the semi-dilute regime. However, Prabhakar et al.[66] acknowledge that similar models are needed for stretched chains in a good solvent, and there is an utter lack of extensional rheology data for the intrinsically semi-dilute, unentangled solutions. In this contribution, we analyze capillary thinning dynamics and extensional rheology response of intrinsically semi-dilute, unentangled solutions ($1 < c/c^* < c_e/c^*$) to obtain measurements of extensional relaxation time for five different molecular weights.

Quantitative analysis of the capillary-thinning and pinch-off dynamics of a stretched liquid bridge[48,49,51,52,56] is used in the Capillary Break-up Extensional Rheometer (CaBER).[11,63,95] As the stretched bridge is formed by applying a discrete step-strain to a drop placed between two parallel plates, and separating the plates requires a finite time, the CaBER (and devices based on step-strain) are impractical for accessing the pinch-off dynamics of low viscosity ($\eta < 20$ mPa · s), low elasticity ($\lambda < 1$ ms) fluids, including aqueous polymer solutions. We recently[12] showed that Dripping-onto-Substrate (DoS) rheometry protocols that involve visualization and analysis of capillary-driven thinning and pinch-off dynamics of a columnar neck formed between a nozzle and a sessile drop can be used for measuring extensional viscosity and extensional relaxation time for highly dilute, aqueous polymer solutions (low shear viscosity $\eta \leq 2$ mPa · s and sub-millisecond relaxation times). Measurement of such short relaxation times are inaccessible in most commercially-available shear and extensional rheometers, although a few measurements of such low relaxation times have been reported recently[10,12,96] (e.g., by using a jetting-based rheometer). In this contribution, we use DoS rheometry for examining how concentration-dependent extensional viscosity and extensional relaxation time change with polymer molecular weight (extensibility) and concentration (degree of overlap) for intrinsically semi-dilute solutions. The experimental datasets presented here elucidate how variation in concentration and molecular weight of polymers affects processability and processing time scale for printing, spraying, and coating applications especially in cases where finite time pinch-off is highly desirable.

MATERIALS AND METHODS

Aqueous solutions of poly(ethylene oxide) (PEO; Sigma-Aldrich) of five molecular weights (average molecular weights are 300, 600, 1000, 2000 and 5000 kg/mol) were prepared by slowly adding powdered polymer to deionized water. The solutions were placed on a roller for several days to ensure that mixing was homogeneous, and to minimize chain break-up associated with high shear rate mixing flows. The concentration of solutions reported in this study for each molecular weight ranges from $1 < c/c^* < c_e/c^*$, although we have also carried out extensive characterization for dilute solutions.[12] In shear rheology, solutions are considered dilute if $c/c^* < 1$, and for such solutions, the concentration-dependent solution shear viscosity $\eta = \eta_s(1 + c/c^*)$ is comparable to solvent viscosity, η_s.

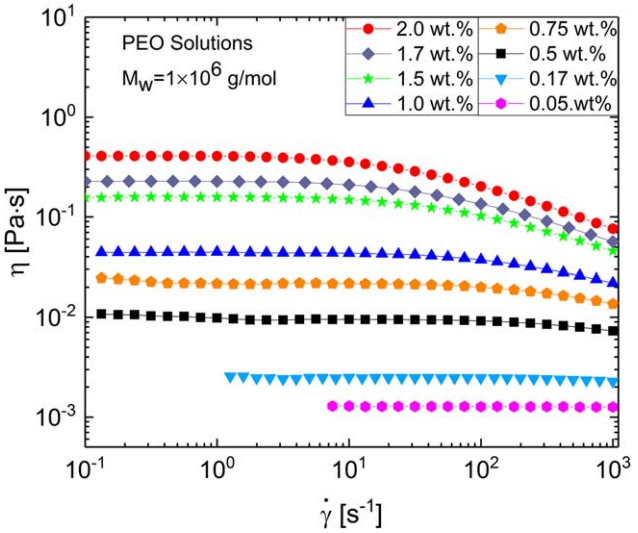

FIGURE 1 Steady shear viscosity as a function of shear rate for a range of aqueous PEO solutions ($M_w = 10^6$ g/mol, with $c^* = 0.17$ wt %). The measurements were carried out on an Anton Paar MCR 302 (WESP) using double gap Couette geometry at 25 °C.

The shear rheology response of the polymer solutions was characterized using a concentric cylinder (double gap) Couette cell on an Anton Paar MCR 302 Rheometer (torque range 10^{-5}–200 mN-m), and a representative dataset is shown in Figure 1 for aqueous PEO solutions ($M_w = 10^6$ g/mol, with $c^* = 0.17$ wt %). The values measured here and the concentration-dependent response is similar to behavior reported in literature.[54,83] All experiments were conducted at 25 °C. The steady shear viscosity, $\eta(\dot{\gamma}) \equiv \tau/\dot{\gamma}$ is computed from the measured shear stress, τ resulting from a specified applied shear rate, $\dot{\gamma}$. The dilute aqueous PEO solutions seem to show a rate-independent viscosity value for the entire shear rate range. In contrast, the semi-dilute solutions (for $c > c^* = 0.17$ wt. %; see Fig. 1) display shear thinning. As the polymer concentration is increased, the onset of shear thinning shifts to lower shear rates, as the shear relaxation time for semi-dilute polymer solutions increases with concentration.

Critical overlap concentration and Zimm relaxation times values with varying molecular weights of PEO are provided in Table 1. The estimates are based on molecular weight listed by the supplier, and while making quantitative comparisons with datasets, we must account for relative polydispersity of these commercial polymer samples. The critical overlap concentrations, c^*, were calculated using the formula $c^*[\eta] \approx 1$ and the Mark-Houwink-Sakurada equation: $[\eta] = KM_w^a$. Here, intrinsic viscosity, $[\eta]$ depends on molecular weight of the polymer and the values of coefficient $K = 1.25 \times 10^{-2}$mL/g and the exponent $a = 0.78$ are listed in the polymer handbook data.[97] The Zimm relaxation time values are estimated using $\lambda_z = \frac{1}{\zeta(3\upsilon)} \frac{[\eta]\eta_s M_w}{RT}$. The pre-factor can be approximated by the Riemann zeta function $F \simeq 1/\zeta(3\upsilon) = 1/\sum_{i=1}^{\infty}(1/i^{3\upsilon})$ in which υ represents the solvent quality exponent, and it varies from $\upsilon = 0.5$ for an ideal chain in a theta solvent to

TABLE 1 Properties of PEO Solutions for Four Different Average Molecular Weights of Polymer

Molecular Weight, M_w (g/mol)	Critical Overlap Concentration, c^* (wt %)	Number of Kuhn Segments, N_K	Estimated Zimm Relaxation Time, λ_z (ms)
3×10^5	0.43	2784	0.01
6×10^5	0.25	5568	0.04
1×10^6	0.17	9280	0.1
2×10^6	0.1	18560	0.35
5×10^6	0.048	46400	1.8

$\nu = 0.588$ for a coil in the good solvent.[86] For the Kuhn chain, the maximum extension or finite extensibility limit of a chain can be estimated by extensibility $L \equiv R_{max}/\langle R_o^2\rangle^{1/2} = N_K{}^{1-\nu}$ that contrasts the contour length of the chain R_{max} as a measure of the maximum size to which a chain can be stretched, to the mean square end-to-end distance $\langle R_o{}^2\rangle$ as an estimate for unperturbed coil size. For this study, we selected aqueous PEO solutions to examine the response of model flexible polymers in good solvent with reasonably high extensibility. The high extensibility polymer solutions show a well-defined elastocapillary regime, allowing us to measure concentration-dependent extensional relaxation time.

Pinch-off dynamics and extensional rheology response were characterized using DoS experimental protocols that were developed and described in our previous contributions,[12,13] where we showcased the versatility of DoS rheometry by characterizing and contrasting the pinch-off dynamics of a wide spectrum of simple and complex fluids: water, printing inks, dilute polymer solutions, emulsions, yield stress fluids, food materials (including honey, chocolate syrup, mayonnaise, ketch-up, and egg yolk), and cosmetics (shampoo, handcream, and conditioner). We showed that the same scaling laws and stress balances apply for DoS rheometry as are used for analysis with CaBER and other capillary-thinning measurements.[9–11,24,26,47–49,79–82] The experimental system for DoS rheometry includes an imaging system and a dispensing system, as shown in Figure 2.

A syringe pump connected to a nozzle is used for depositing a discrete volume of fluid is delivered at a flow rate, Q. Relatively low shear rates ($< 1\ s^{-1}$) are encountered within the stainless steel nozzle (inner and outer diameters, $D_i = 0.838$ mm and $D_0 = 2\,R_0 = 1.27$ mm) for flow rate $Q = 0.02$ mL/min used in this study, and as the estimated Zimm relaxation time for each molecular weight is $\lambda_Z < 10$ ms, the relaxation rate within nozzle is much faster than deformation rate. The volume is then deposited onto a glass substrate placed at a fixed distance H below the nozzle. In contrast, much higher shear rates values ($>10^3\ s^{-1}$) and a pre-stretch are quite typical within the nozzle during jetting-based rheometry studies.[10,38] We have noted before[12,13] that slow release of drops onto a partial wetting substrate (spreading parameter $S < 0$ and contact angle $\theta < 90°$) helps to decouple the neck thinning dynamics from the drop spreading dynamics. If needed, the contact line of the sessile drop can be pinned by using a cylindrical plate as a substrate, emulating the CaBER configuration. A stretched liquid bridge created between the nozzle and a sessile drop on substrate (see Fig. 2) undergoes capillary-driven instability and thinning followed by the pinch-off at the necked region of fluid (see Figs. 3 and 4 for montages). Movies of this self-thinning process for a range of semi-dilute polymer solutions were captured at a rate of 500–8,000 frames per second. The imaging system consists of a light source, a diffuser and a Photron Fastcam SA3 high-speed camera with an addition of a Nikkor 3.1× zoom lens (18–50 mm) and an additional super macro lens.

The DoS videos were analyzed using ImageJ[98] and MATLAB with specially written codes for edge detection, and determination of neck radius for analyzing thinning and pinch-off dynamics. Radius evolution datasets are obtained using the MATLAB code, and the step-by-step description of the analysis is included in the supplementary document online. Since aqueous solutions wet metal nozzle(s) used in this study, the outer diameter of nozzle, D_o is used for scaling the neck diameter. The nozzle size is also used for determining the

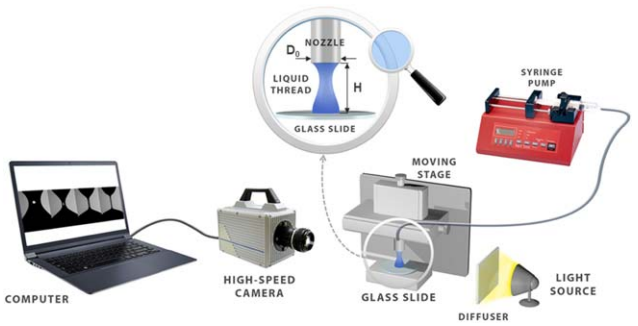

FIGURE 2 Schematic for DoS Rheometry. The set-up includes an imaging system and a dispensing system. The dispensing system includes a syringe pump that releases a finite volume of fluid through a nozzle placed height H above the clean glass substrate. Size of the nozzle used in this study was D_0=1.27 mm and the aspect ratio selected was $H/D_0 \approx 3$. The imaging system includes a light source, a diffuser and a high-speed camera (with magnifying lenses) connected to a laptop for visualizing and recording the capillary thinning and pinch-off dynamics of the liquid neck formed by dispensing a discrete amount of fluid onto a substrate.

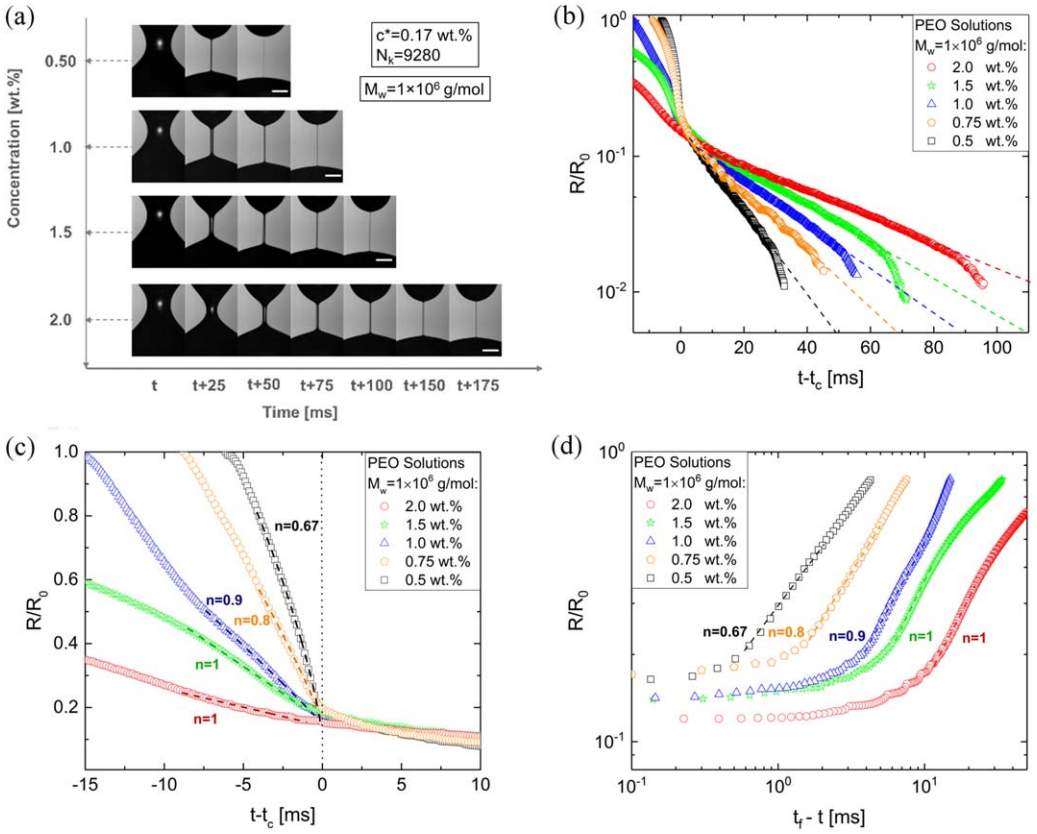

FIGURE 3 Characterizing capillary-driven thinning and pinch-off dynamics of semi-dilute PEO polymer solutions ($M_w = 1 \times 10^6$ g/mol) using DoS rheometry technique. (a) Sequence of images show thinning dynamics for four concentrations of semi-dilute aqueous PEO solutions acquired using a high-speed camera. Time step between the images is Δt=25 ms and the scale bar is 0.5 mm. The neck shape evolves into the cylindrical shape associated with elastocapillary thinning. Movies obtained for 1 and 1.5% PEO are included as supplementary data online. (b) Neck radius evolution in time data for semi-dilute polymer solutions displayed with the onset of elastocapillary regime matched. Radius evolution shows three distinct regimes and the intermediate elastocapillary regime that appears linear on the semi-log plot is analyzed and fit with eq 4. The fits yield a measurement of extensional relaxation time (see values listed in Table 2). Increasing polymer concentration leads to a longer pinch-off time, and a longer extensional relaxation time. (c) Neck radius evolution data before the onset of elastocapillary regime shows a power law dependence on time, and the exponent increases from 2/3 (IC) to 1 (VC) commensurate with an increase in solution viscosity. (d) Scaled radius evolution plotted with time axis shifted is shown on a double log plot to highlight the change in scaling exponent in the initial regime, that is, before the onset of elastocapillary thinning behavior. The power law fits $R/R_0 = A(t_f - t)^n$ for each dataset show that the initial regime exhibits IC behavior with $n = 2/3$ for low shear viscosity solutions ($\eta < 10$ mPa · s) and VC exponent of $n = 1$ is obtained for higher viscosity solutions.

absolute pixel size per unit length. The typical size of symbols chosen for all the radius evolution plots included in this article is of the same order as the error ($\sim$ 10 μm) estimated by accounting for the resolution of the imaging systems and the analysis protocols.

RESULTS AND DISCUSSION

Concentration-Dependent Pinch-off Dynamics of Unentangled, Semi-Dilute PEO Solutions

The capillary thinning and pinch-off dynamics of representative semi-dilute solutions ($c = 0.5$, 1.0, 1.5, and 2.0 wt %) of a high molecular weight PEO ($M_w = 10^6$ g/mol, with $c^* = 0.17$ wt %) shown in Figure 3(a) were acquired using DoS rheometry set-up. The necks formed between a nozzle and a substrate are cylindrical slender filaments, characteristic of high viscosity or high elasticity fluids,[11,99] and distinct from conical necks associated with inviscid or power law fluids.[100] The first image in the sequence for each concentration [see Fig. 3(a)] represents the specific moment at which the neck radius is half of the nozzle radius $R \approx 0.5R_0$. Comparison of the image sequences illustrates that the thinning rate decreases and pinch-off time increases with an increase in concentration. Neck radius evolution over time plots shown in Figure 3(b) show the concentration-dependent delay in pinch-off. Since the radius evolution datasets show at least two distinct regimes, the datasets are all shifted such that the first transition point t_c overlaps for all five concentrations plotted here. The initial neck-thinning dynamics are determined by interplay of capillary, viscous, and inertial

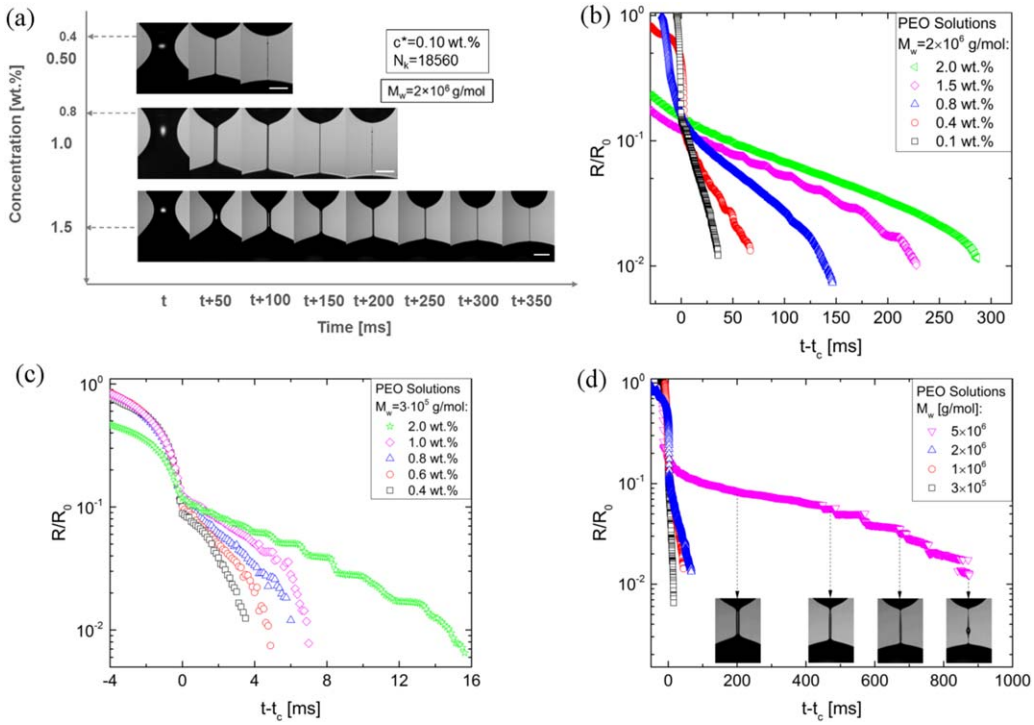

FIGURE 4 Characterization of capillary-driven thinning and pinch-off dynamics of unentangled, semi-dilute solutions of PEO. (a) Sequence of images acquired using the DoS rheometry technique for three different concentrations for $M_w = 2\times10^6$ g/mol; $N_K = 18{,}560$. The time interval between snapshots is $\Delta t = 50$ ms, and the scale bar is 0.5 mm. (b) Neck radius evolution in time data for semi-dilute PEO solutions ($M_w = 2\times10^6$ g/mol) displays a mild transition to the intermediate elastocapillary regime; the data is shifted to highlight the transition zone, and show how pinch-off time increases with an increase in polymer fraction. (c) Neck radius evolution in time data for lower molecular weight PEO solutions ($M_w = 3\times10^5$ g/mol) shows that pinch-off time < 20 ms. (d) Increasing molecular weight results in more delayed pinch-off. The snapshots shown are for thinning neck of PEO solution with $M_w = 5\times10^6$ g/mol, $c/c^* \approx 4.2$. The data included here is for $M_w = 3\times10^5$ g/mol, $c/c^* \approx 4.65$, $M_w = 1\times10^6$ g/mol, $c/c^* \approx 4.4$, and $M_w = 2\times10^6$ g/mol, $c/c^* \approx 4$.

stresses. Additional viscoelastic stresses contributed by polymers play a role after t_c as detailed below.

For low viscosity fluids, the initial neck thinning dynamics are dominated by inertial and capillary stresses, leading to the following inertio-capillary (IC) scaling[24,27] formula:

$$\frac{R(t)}{R_0} = 0.8\left(\frac{t_f - t}{t_R}\right)^{\frac{2}{3}} \tag{1}$$

Here, t_f represents the pinch-off time for an inviscid fluid obtained by fitting eq 1. The IC time or Rayleigh time $t_R = (\rho {R_0}^3/\sigma)^{1/2}$ is the characteristic time-scale for IC thinning[2,5,6] and is associated with oscillation frequency of a drop of mass $\rho {R_0}^3$ acted upon by scaled restoring force set by surface tension (acts like an "effective spring constant"). We have shown before[12] that the IC thinning is observed for the solvent as well as in the initial regime, for dilute PEO solutions (same $M_w = 10^6$ g/mol) where solution shear viscosity is less than twice water viscosity. As shown in Figure 3(c), the IC scaling can be observed up to concentration of $c = 0.5\%$ by weight. Thus, we find that the initial neck radius evolution exhibits IC thinning for $c/c^* \leq 3$ in aqueous PEO solutions with $M_w = 10^6$ g/mol, and the radius evolution can be described using eq 1 though the pinch-off time for these polymer solutions is significantly longer than the value of t_f obtained from the fit. Beyond a critical time t_c ($t_c \neq t_f$) neck thinning behavior displays elastocapillary scaling for dilute polymer solutions, as discussed later in the article.

However, for higher viscosity fluids, the radius evolution is primarily determined by the interplay of viscous and capillary stresses leading to the Papageorgiou's[25,26] visco-capillary (VC) scaling:

$$\frac{R}{R_0} = 0.0709\frac{\sigma}{\eta R_0}(t_p - t) = 0.0709\left(\frac{t_p - t}{t_{vc}}\right) \tag{2}$$

Indeed the linear decrease in radius can be used for determining viscosity of a Newtonian fluid as long as surface tension is known. The characteristic time scale for VC thinning is called VC time $t_{vc} = \eta R_0/\sigma$ and t_p refers to the pinch-off time. The relative importance of viscous and IC effects can be evaluated by computing Ohnesorge number, $Oh = t_{vc}/t_R = \eta/\sqrt{\rho\sigma R_0}$. IC effects are observed for $Oh \ll 1$ and for aqueous PEO solutions ($M_w = 10^6$ g/mol), the dilute solutions satisfy the criteria. On increasing polymer concentration, shear viscosity increases and the viscous stresses become comparable to inertial and

TABLE 2 Zero Shear Viscosity, Extensional Relaxation Time, and Steady Terminal Extensional Viscosity Values as a Function of Concentration for Semi-Dilute Aqueous PEO Solutions ($M_w = 10^6$ g/mol, with $c^* = 0.17$ wt %)

Concentration (wt. %)	η_0 (Pa · s)	λ_E (ms)	G_E (Pa)	η_E^∞ (Pa · s)
0.5	0.01	4.66 ± 0.23	0.91	32
0.75	0.022	6.59 ± 0.1	0.6	38
1.0	0.044	9.36 ± 0.39	0.58	41
1.5	0.16	12.02 ± 1.03	0.64	45
2.0	0.41	16.51 ± 0.68	0.48	73

capillary stresses. While the VC scaling is observed clearly for higher concentrations [see Fig. 3(c,d)] where $Oh > 1$, we report here that for the fluids of intermediate viscosity values, a plethora of scaling exponents can be observed.[27] Figure 3(d) shows radius evolution for the initial regime plotted using a shifted scale on a log-log axis to highlight the increase in power law index from $n = 2/3$ to $n = 1$ when $R/R_0 = A(t_f - t)^n$ is used for fitting the data for each concentration (e.g., for VC fits, $t_p = t_f$ and $n = 1$).

Beyond the transition point, all semi-dilute polymer solutions show a pronounced elastocapillary behavior. The elastocapillary thinning dynamics can be described using the following expression based on a theory developed by Entov and Hinch[65]:

$$\frac{R(t)}{R_0} = \sum_i \left(\frac{g_i R_0}{2\sigma}\right)^{1/3} \exp\left[-t/3\lambda_i\right] \quad (3)$$

Here g_i, λ_i are the modulus and relaxation time that correspond to the ith mode of the relaxation spectrum.[65] For many polymer solutions,[11,65] the elastocapillary response can be captured reasonably well by a single exponential relaxation function, using the following approximate equation[11,65]:

$$\frac{R(t)}{R_0} \approx \left(\frac{G_E R_0}{2\sigma}\right)^{1/3} \exp\left[-t/3\lambda_E\right] \quad (4)$$

where R_0, G_E, and λ_E are the initial radius of the configuration, apparent elastic modulus, and the extensional relaxation time, respectively. When radius evolution over time is plotted on a semi-log plot (see Fig. 3), the elastocapillary regime displays as a straight line. The lifetime of the elastocapillary regime and the total time for break-up increase with an increase in the polymer concentration. Nevertheless, the overall pinch-off time is only of the order of 100 ms. Though CaBER measurements are possible for elastocapillary regime for some of the semi-dilute polymer solutions, the onset of the elastocapillary behavior and the regime before it are typically not captured. The concentration-dependent λ_E values obtained from the fits shown in Figure 3 ranges from 3.5 to 16.5 ms for the semi-dilute PEO solutions ($M_w = 1\times10^6$ g/mol). The λ_E values are 35–165 times greater than the estimated value for Zimm relaxation time, $\lambda_z = 0.463([\eta]\eta_s M_w/RT) = 0.1$ ms.

For these PEO solutions ($M_w = 1\times10^6$ g/mol) that if the time axis is rescaled with corresponding extensional relaxation time for each concentration, the radius evolution profile overlaps for the elastocapillary regime. However, as thinning proceeds towards pinch-off, the accumulated strain can stretch the polymer chains to their finite extensibility limit. In the last stage, we notice that the capillary thinning behavior departs from the exponential thinning regime [illustrated using dashed line in Fig. 3(b)]. Before pinch-off, radius displays a linear decrease with time, characteristic of a VC thinning behavior (see eq 2), both strain and strain rate increase dramatically in this regime. The effective viscosity of the thinning filament is much higher than pure solvent or solution shear viscosity, as the steady terminal extensional viscosity is reached for highly stretched chains.[48,49,65] Table 2 lists the zero shear viscosity values (from data displayed in Fig. 1), average extensional relaxation time values obtained by fitting at least three different radius evolution plots, and steady terminal extensional viscosity values obtained from the finite extensibility regime (and shown in Fig. 5) for semi-dilute aqueous PEO solutions ($M_w = 10^6$ g/mol, with $c^* = 0.17$ wt %). The corresponding G_E values are also shown for the dataset used for computing extensional viscosity data included in Figure 5. The finitely extensible models (FENE-P model) predict the change from elastocapillary to effectively VC regime, and predict that fully stretched macromolecules in solution behave like a dilute suspension of rigid rods that increases the total effective viscosity of the fluid.[101,102] In practice, the measured terminal extensional viscosity values are always lower than the theoretical limit, as steady state values are obtained before all the coils are fully stretched.[48,49]

Influence of Molecular Weight on Pinch-off Dynamics of Semi-Dilute PEO Solutions

Increase in pinch-off time with an increase in polymer concentration is also observed for semi-dilute aqueous PEO solutions prepared with four other molecular weights, listed in Table 1. Representative data is shown in Figure 4(a,b) for $M_w = 2\times10^6$ g/mol and Figure 4(c) for lower molecular weight solution ($M_w = 3\times10^5$ g/mol). Increase in overall solution shear and extensional viscosity due to the increase in polymer molecular weight (for the same c/c^* values) results in slowing down of capillary-driven thinning, and therefore pinch-off times for $M_w = 2\times10^6$ g/mol solutions [Fig. 4(b)] are much longer than those observed for $M_w = 1\times10^6$ g/mol [in Fig. 3(b)]. The typical pinch-off time for semi-dilute solutions of the lowest molecular weight polymers studied here ($M_w = 3\times10^5$ g/mol) is < 20 ms [see Fig. 4(c)]. The measurement of elastocapillary response for such systems cannot be obtained using CaBER as the pinch-off time is shorter than the typical time needed (~50 ms) for creating a stretched liquid bridge by applying step-strain to fluid placed between two parallel plates (see Rodd et al.[95] for a detailed discussion). Though such measurements are possible with ROJER or the jetting-based rheometer,[10,103] high shear rates within the nozzle can perturb the chains. In both CaBER and ROJER, the initial deformation and preshear

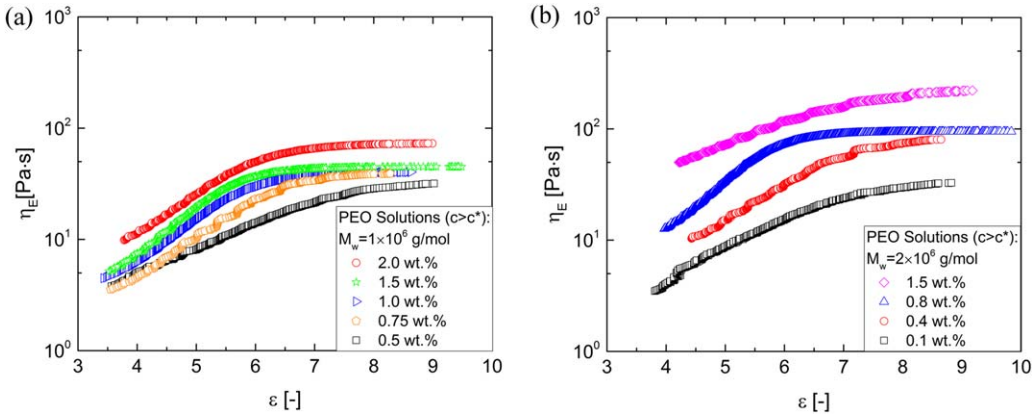

FIGURE 5 Transient extensional viscosity and terminal steady extensional viscosity as a function of Hencky strain. Aqueous semi-dilute PEO solutions with (a) $M_w = 1 \times 10^6$ g/mol and (b) $M_w = 2 \times 10^6$ g/mol, respectively, show a pronounced strain-hardening behavior. At high strains, the steady, terminal extensional viscosity values are obtained, that increase proportionally with molecular weight and polymer concentration.

applied can influence the measurement of extensional relaxation time and extensional viscosity values.[10,13,33,57,63,65,103] The influence of extensibility on overall pinch-off dynamics is illustrated best by contrasting the pinch-off dynamics of four solutions with a similar degree of overlap ($c/c^* \approx 4$) but different molecular weights, as shown in Figure 4(d). The datasets show that high M_w, highly extensible polymers are detrimental to achieving high printing speeds. However, due to the delayed pinch-off, high extensibility polymers serve as ideal additives for improving the spinnability of polymer solutions or particle-polymer dispersions.[40,41]

For dilute solutions, the neck radius evolution displays IC thinning, followed by a sharp transition into an elastocapillary regime, indicative of an underlying coil-stretch transition. In semi-dilute solutions, (see Figs. 3 and 4), a sharp transition is still observed at the lowest concentrations. However, the transition becomes less sharp as the polymer concentration is increased, implying that the coil-stretch transition becomes milder. Experiments with the filament stretching extensional rheometer[104,105] and recent Brownian dynamics simulations[66,67] carried out at Monash also demonstrate that both coil-stretch transition, and coil-stretch hysteresis are milder above the overlap concentration. Recent experiments on extensional flows of fluorescently labeled DNA chains in a semi-dilute solution, visualized in cross-slot geometry, also show a milder coil-stretch transition.[106] Increase in interchain interactions, a broader distribution of conformational states, screened hydrodynamic interactions, and lower fractional extension all could lead to the observed milder coil-stretch transition. Finally, in the last stage of neck thinning, beads-on-a-string structures[10,55,81,104,107–110] appear for many solutions, and the iterated stretching in presence of such beads, is registered in datasets of radius evolution as stepwise thinning shown in Figure 4(d).

Extensional Viscosity of Aqueous Semi-Dilute Polymer Solutions

In the elastocapillary and finite extensibility regime, the primary contributions to stresses within a thinning neck are from elastic stresses $\eta_E\dot{\varepsilon}$ contributed by polymer stretching and orientation, and capillary stresses σ/R that increase with decrease in filament radius.[11,65] The extensional viscosity values can be obtained from the radius evolution data, by using the following formula:

$$\eta_E = \frac{\sigma}{\dot{\varepsilon}(t)\,R(t)} = \frac{\sigma}{-2\mathrm{d}R(t)/\mathrm{d}t} \tag{5}$$

The values of extension rates $\dot{\varepsilon} = -2d\ln R(t)/dt$ for different aqueous PEO solutions are calculated from the radius evolution plots. During the elastocapillary phase of the thinning process, a homogeneous extensional flow with a constant and self-selected extension rate (dependent on the extensional relaxation time) is established within the neck. Though extension rate is constant, the Hencky strain or the total accumulated strain in the liquid filament, $\varepsilon = 2\ln\left(\frac{R_0}{R(t)}\right)$ increases. The extensional viscosity variation with increasing strain is displayed in Figure 5 for semi-dilute PEO solutions of different two molecular weights ($M_w = 1\times10^6$ g/mol and $M_w = 2\times10^6$ g/mol).

Extensional viscosity increases with both polymer concentration and molecular weight, and significant strain hardening is observed even for the solutions that exhibit shear thinning behavior (see Fig. 1). The absolute values of extensional viscosity of the intrinsically semi-dilute polymer solutions are 10^2–10^4 times higher than their zero shear viscosity (see Table 2 and Fig. 1), and this enhancement contributes to the delayed pinch-off. During elastocapillary thinning phase, a transient extensional viscosity, $\eta^{\dagger}_E(\dot{\varepsilon}, \varepsilon, t)$ is measured using the DoS rheometry technique. The extension rate remains constant, while Hencky strain grows linearly in time. Furthermore, the extension rate realized for each polymer concentration is different, even though the Wiessenberg number (or the ratio of extension rate to the extensional relaxation rate) has a constant value of 2/3. The extensional flow field results in progressive stretching and orientation of the polymer in solution. In the final stage, as the neck radius thins linearly with time, the extension rate increases and diverges. The presence of the last regime allows the measurement of

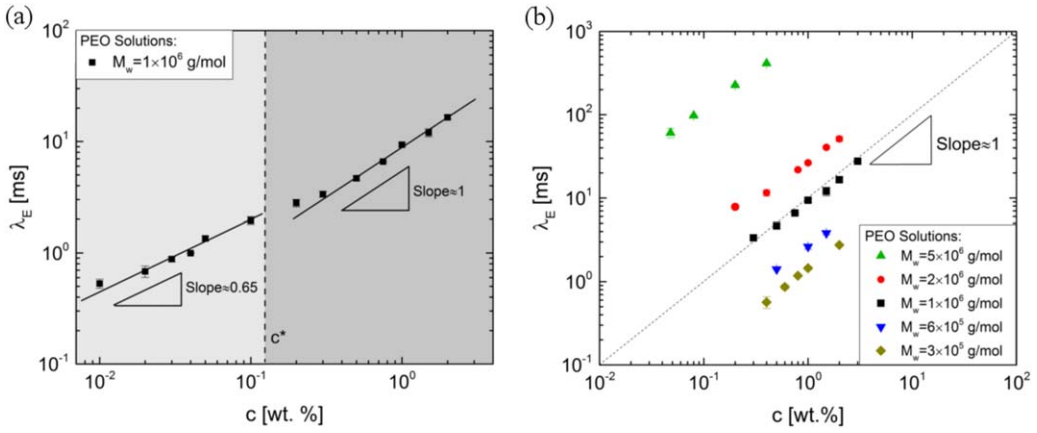

FIGURE 6 Extensional relaxation time λ_E for aqueous PEO solutions obtained using DoS experimental protocol. (a) The extensional relaxation time datasets for PEO solutions ($M_w = 10^6$ g/mol). As indicated in the figure, their concentration dependence shows two distinct regimes. (b) Extensional relaxation time λ_E extracted using DoS extensional rheometry protocol as a function of concentration for five molecular weights of aqueous PEO. All concentrations shown are considered semi-dilute based on critical overlap concentration c^* calculations for unperturbed coils.

terminal steady extensional viscosity value that is independent of both extension rate and strain. The terminal steady extensional viscosity value is arguably a true material response[48,49] that depends on both molecular weight and polymer concentration, but not on extension rate or accumulated strain. The terminal steady extensional viscosity values are reached before all the chains are completely stretched out.[49,111,112]

Extensional Relaxation Time of Unentangled Semi-Dilute Polymer Solutions

Extensional relaxation time (λ_E) values obtained by fitting the elastocapillary regime [see Figs. 3(b) and 4(b–d)] with eq 4 are plotted as a function of concentration for both dilute and semi-dilute PEO solutions ($M_w = 1\times10^6$ g/mol) as shown in Figure 6(a). The extensional relaxation time shows two distinct regimes: the concentration-dependent scaling $\lambda_E \sim c^m$ has exponent $m \approx 0.65$ for dilute solutions ($c/c^* < 1$), whereas $m \approx 1$ for intrinsically semi-dilute, unentangled solutions ($1 < c/c^* < c_e/c^*$). Extensional relaxation time values for aqueous semi-dilute PEO solutions of five different molecular weights obtained by DoS rheometry are displayed in Figure 6(b). The concentration-dependent relaxation time data shows the same exponent $m \approx 1$, though the absolute values of the extensional relaxation time increase as molecular weight or extensibility is increased. For PEO solutions dissolved in water, Arnolds et al.[83] found that exponent of $4/3 \pm 1/3$ in neck thinning experiments conducted with CaBER for semi-dilute polymer solutions. As bulk of the data reported in Arnolds et al.[83] were acquired for $c/c^* > 10$ both entanglement effects and the influence of shear thinning lead to somewhat higher exponent (and higher error bars for slope and data displayed in their plots). Likewise, Clasen's measurements of extensional relaxation time of semi-dilute solutions of polystyrene (PS) in diethyl phthalate primarily include datasets for $c/c^* > 8$ or intrinsically entangled solutions.[113] The datasets included in Figure 6(b) are chosen to illustrate how extensional relaxation time for intrinsically semi-dilute unentangled solutions show linear concentration dependence, and the behavior is quite distinct from solutions with $c/c^* < 1$.

Several researchers have discussed the exponent for concentration-dependent increase of extensional relaxation time for dilute polymer solutions ($c/c^* < 1$), obtaining values ranging from $m = 0.65$ for PEO solutions in water and glycerol/water[54] using dripping, $m=0.58$ for PS in the relatively good solvent DEP and $m=0.89$ PS dissolved in the near theta solvent of styrene oligomer[79] using CaBER and $m = 0.65$ using DoS rheometry for aqueous PEO solutions.[12] Even for relatively low concentrations ($c/c^* < 0.1$), the extensional relaxation time values exceed the values predicted by Zimm theory. Near the overlap concentration ($c/c^* < 1$), measured extensional relaxation time values show a power law in their concentration dependence, that is distinct from the linear concentration-dependence $\lambda(c)=\lambda_{RZ}(1+k_H[\eta]c)$, where k_H is the Huggins constant, anticipated by Muthukumar and Freed.[114] However, even if polymer coils are initially non-overlapping (as expected in dilute solution), as stretched chains can overlap, several authors[54,67,79,115] invoke the blob theory or composite Rouse-Zimm model developed for intrinsically unentangled semi-dilute solutions for describing the dynamics of partially overlapping stretched polymer coils, as is discussed next.

The blob theory, as originally devised for intrinsically semi-dilute solutions, assumes that on length scales larger than the correlation length ($\xi_h \approx \xi$, hydrodynamic comparable to EV screening length), the dynamics are many-chain like, both EV and hydrodynamic interactions are screened, and Rouse-like dynamics are followed. Relaxation time on these length scales can be described using Rouse model according to equation $\tau_{chain} \approx \tau_\xi \left(\frac{N}{g}\right)^2 \approx \frac{\eta_s}{kT}\xi^3\left(\frac{N}{g}\right)^2$ and the number of monomers in the correlation blob is $g \approx \phi\left(\frac{\xi}{b}\right)^3 \approx \phi^{-1/(3\nu-1)}$. The volume fraction ϕ is related to the concentration c' in

mass/volume by the expression $\phi = c' N_K b_K^3 N_A / M_w$. By combining these two expressions, the resulting expression for concentration dependent relaxation time becomes:

$$\tau_{chain} \approx \tau_\xi \left(\frac{N}{g}\right)^2 \approx \frac{\eta_s}{kT}\xi^3 \left(\frac{N}{g}\right)^2 \approx \frac{\eta_s b^3}{kT} N^2 \phi^{(2-3\nu)/(3\nu-1)} \quad (6)$$

The exponent that describes concentration dependence is $m = (2-3\upsilon)/(3\upsilon-1) \cong 0.31$ for good solvents (EV interactions included) and $m = (2-3\upsilon)/(3\upsilon-1) \cong 1$ if EV interactions are screened or absent.

Water is considered to be a good solvent for PEO and it is therefore, expected that relaxation time of the semi-dilute aqueous PEO solutions would show a concentration dependence with the exponent, $m = 0.31$. However, as seen in Figure 6(a), relaxation time extracted from DoS extensional rheometry experiments, λ_E, shows $m = 0.65$ for $c/c^* < 1$ and similar values are obtained when experiments utilize dilute polymer solutions.[12,48,49,54,79] In a previous contribution on extensional relaxation times for dilute PEO solutions, we argued that as the EV interactions will be screened only partially for stretched chains, the extensional relaxation time is likely to be a geometric mean of the exponent for good and theta solvent. By defining a monomer relaxation time as $\lambda_o \approx \eta_s b^3/kT$, this leads to a relationship of the form $\lambda_E \approx \lambda_o N^2 \phi^{0.65}$ that seems to quantitatively capture the concentration dependence observed for dilute solutions (and for similar literature data[10,28,29,54]). For intrinsically semi-dilute, unentangled solutions, the shear relaxation time is expected to show $m = 0.31$ in good solution and $m = 1$ in a theta solvent. Following the arguments of de Gennes,[89,91] Pincus[93,94] and Brochard-Wyatt et al.[73] that outline relaxation dynamics for single stretched chains using tension blob concepts, we posit that the stretching of polymer coils leads to progressive screening of EV interactions and due to conformational anisotropy, stretching also alters the local hydrodynamic interactions. For stretched polymer chains of intrinsically semi-dilute solutions, the EV interactions are screened on all length scales irrespective of the solvent quality. Thus, the exponent approaches value $m = 1$ for a "theta solvent" as is observed experimentally (see Fig. 6).

The extensional relaxation time data for aqueous semi-dilute PEO solutions with molecular weights of 6×10^5, 1×10^6, and 2×10^6 g/mol provide a self-consistent estimate for the $\lambda_E/\lambda_o N^2$), and the three datasets yield the monomer relaxation time λ_o values of 1.18, 1.24, and 1.38 ns, respectively. The values are marginally higher than the value estimated using $\lambda_o \approx \eta_s b^3/kT = 0.29$ ns, and the extension-rate dependent values obtained from neutron spin echo measurements[116] (segmental relaxation time of 117 ps was reported for an extension rate of 4 s^{-1}). Thus, it is possible to make an estimate for Zimm relaxation time using $\lambda_Z \approx \lambda_o N^{3\upsilon}$ as well as Rouse relaxation time using λ_o values extracted from DoS rheometry data. We find that for the aforementioned three molecular weights, the estimates for Zimm time obtained by using monomeric friction values extracted from DoS rheometry measurements are of the same order of magnitude as those obtained using the formula $\lambda_z = \frac{1}{\zeta(3\nu)}\frac{[\eta]\eta_s M_w}{RT}$. However, other factors like amplified concentration fluctuations, possible role of topological constraints, conformational anisotropy and the resulting influence on the overall drag coefficient and on the relaxation dynamics, are not captured by eq 6, and these warrant further investigation.[66,67,84,85,106,117,118]

CONCLUSIONS

Capillary-driven thinning and pinch-off dynamics of intrinsically semi-dilute, unentangled PEO solutions of different molecular weights were investigated using DoS rheometry technique. Our experimental results show that the macromolecular dynamics in intrinsically semi-dilute solutions exhibit concentration-dependent response to extensional flows that is quite distinct from nominally dilute polymer solutions that can exhibit some degree of overlap on stretching. Pinch-off time increases with an increase in concentration for the intrinsically semi-dilute polymer solutions (with concentrations above a critical overlap concentration, c^* computed using the equilibrium coil size). In contrast to the very pronounced IC behavior observed for the initial neck thinning for the highly dilute, aqueous PEO solutions, the initial thinning dynamics of the semi-dilute solutions displays IC exponent (2/3) for lowest concentrations and VC scaling (exponent, $n = 1$) at the highest concentrations explored in this study. However, a plethora of intermediate exponents ($2/3 < n < 1$) are observed for a range of concentrations. In the initial regime, the interplay of viscosity, inertia, and capillary stresses governs the thinning dynamics. Due to the relatively high extension rates, and accumulated strain realized in extensional flows within the thinning neck, polymers can under-go a coil-stretch transition, and thereafter the thinning dynamics switches to elastocapillary response as the interplay of viscoelastic stresses and capillarity governs the thinning dynamics. Semi-dilute solutions of highly extensible PEO solutions used in the current study display a pronounced elastocapillary regime, but the transition to elastocapillary regime is not as sharp as observed for dilute solutions, implying coil-stretch transition is milder, in agreement with observations made in stagnation flow experiments.

Both extensional relaxation time and extensional viscosity (transient and terminal steady value) of unentangled semi-dilute solutions increase with concentration, and we show that the extensional rheology response of intrinsically semi-dilute solutions is quite distinct from that of dilute solutions. In shear flow of unentangled semi-dilute solutions in good solvent, concentration-dependent variation in relaxation time is expected to display an exponent of $m = 0.31$. However, the extensional relaxation time measured using DoS rheometry increases linearly with concentration, displaying exponent $m = 1$. The observed relaxation time dependence indicates that EV interactions for stretched chains are screened on all length scales and thus, relaxation time scales with concentration linearly as expected for theta solvents. The stretching of

chains can also influence the threshold for observing the effect of entanglements, as well as relative number of entanglements, and such effects become more manifest at higher concentrations.[71,72,106] The possibility of chain entanglements due to stretching of initially unentangled solutions was not considered in the present contribution, and these effects require further investigation using higher concentration solutions. Based on the experimental data from Arnolds et al.[83] and Sachsenheimer et al.[119] for aqueous PEO solutions and Clasen[82] for PS dissolved in DEP, the extensional relaxation time is expected to show a shaper concentration-dependent increase than observed for unentangled dilute and semi-dilute solutions.

Although this study is exclusively focused on the capillary-driven neck thinning, extensional flow fields arise in all realistic processing flows involving converging or diverging channels (enhanced oil recovery[73,120,121] and flows through membranes), mixed flows with strong extensional component (turbulent drag reduction[122–124] and coating flows[125–127]), and flow through nozzles and needles connected wider bore capillaries or syringes, relevant for pumping and liquid transfer applications. Although the transient extensional viscosity relevant for such flows is not captured by the capillary-driven thinning experiments, both extensional relaxation time values and the measured terminal steady extensional viscosity values are material parameters that provide insight into the processing behavior of polymeric complex fluids. Finally, it is hoped that the presented datasets will provide motivation for developing constitutive models that capture and describe the concentration-dependent increase in the value of terminal, steady extensional viscosity values, and the role of extensibility as well as accumulated extensional strain.

ACKNOWLEDGMENTS

The authors acknowledge contribution by Leidy Nallely Jimenez and Yiran Zhang to the development of DoS rheometry protocols. V. Sharma thanks the UIC College of Engineering and the Department of Chemical Engineering for start-up funds, and acknowledges an initiation grant from the Campus Research Board (CRB) at UIC. M. Biagioli participated in the research as an undergraduate student; she is currently pursuing a doctorate in chemical engineering at University of Illinois at Urbana-Champaign.

REFERENCES AND NOTES

1 L. Rayleigh, *Proc. London Math. Soc.* **1878**, *s1–10*, 4–13.

2 L. Rayleigh, *Proc. R. Soc. London* **1879**, *29*, 71–97.

3 S. Chandrasekhar, Hydrodynamic and Hydromagnetic Stability; Oxford University Press: Oxford, **1961**.

4 S. Middleman, *Chem. Eng. Sci.* **1965**, *20*, 1037–1040.

5 S. Middleman, Modeling Axisymmetric Flows: Dynamics of Films, Jets and Drops; Academic Press: San Diego, **1995**.

6 J. Eggers, *Rev. Mod. Phys.* **1997**, *69*, 865–929.

7 J. Eggers, M. A. Fontelos, Singularities: Formation, Structure, and Propagation; Cambridge University Press: Cambridge, UK, **2015**.

8 J. Eggers, E. Villermaux, *Rep. Prog. Phys.* **2008**, *71*,

9 A. L. Yarin, Free Liquid Jets and Films: Hydrodynamics and Rheology; New York, NY: Longman Scientific & Technical, **1993**.

10 V. Sharma, S. J. Haward, J. Serdy, B. Keshavarz, A. Soderlund, P. Threlfall-Holmes, G. H. McKinley, *Soft Matter.* **2015**, *11*, 3251–3270.

11 G. H. McKinley, *Rheol. Rev.* **2005**, 1–48.

12 J. Dinic, Y. Zhang, L. N. Jimenez, V. Sharma, *ACS Macro. Lett.* **2015**, *4*, 804–808.

13 J. Dinic, L. N. Jimenez, V. Sharma, *Lab. Chip.* **2017**, *17*, 460–473.

14 O. A. Basaran, *AIChE J.* **2002**, *48*, 1842–1848.

15 O. A. Basaran, H. Gao, P. P. Bhat, *Annu. Rev. Fluid Mech.* **2013**, *45*, 85–113.

16 S. Kumar, *Annu. Rev. Fluid Mech.* **2014**, *47*, 67–94.

17 Handbook of Atomization and Sprays: Theory and Applications; N. Ashgriz, Ed.; Springer: New York, **2011**.

18 G. F. Christopher, S. L. Anna, *J. Phys. D: Appl. Phys.* **2007**, *40*, R319.

19 S. T. Thoroddsen, T. G. Etoh, K. Takehara, *Annu. Rev. Fluid Mech.* **2008**, *40*, 257–285.

20 S. Gaudet, G. H. McKinley, H. A. Stone, *Phys. Fluids* **1996**, *8*, 2568–2579.

21 X. Zhang, R. S. Padgett, O. A. Basaran, *J. Fluid Mech.* **1996**, *329*, 207–245.

22 O. E. Yildirim, O. A. Basaran, *Chem. Eng. Sci.* **2001**, *56*, 211–233.

23 X. Shi, M. P. Brenner, S. R. Nagel, *Science.* **1994**, 219–219.

24 R. F. Day, E. J. Hinch, J. R. Lister, *Phys. Rev. Lett.* **1998**, *80*, 704–707.

25 D. T. Papageorgiou, *Phys. Fluids* **1995**, *7*, 1529–1544.

26 G. H. McKinley, A. Tripathi, *J. Rheol.* **2000**, *44*, 653–670.

27 J. R. Castrejón-Pita, A. A. Castrejón-Pita, S. S. Thete, K. Sambath, I. M. Hutchings, J. Hinch, J. R. Lister, O. A. Basaran, *Proc. Natl. Acad. Sci. USA* **2015**, *112*, 4582–4587.

28 Y. Christanti, L. M. Walker, *J. Non-Newtonian Fluid Mech.* **2001**, *100*, 9–26.

29 Y. Christanti, L. M. Walker, *J. Rheol.* **2002**, *46*, 733–748.

30 D. W. Bousfield, R. Keunings, G. Marrucci, M. M. Denn, *J. Non-Newtonian Fluid Mech.* **1986**, *21*, 79–97.

31 P. Schummer, K. H. Tebel, *Rheol. Acta.* **1982**, *21*, 514–516.

32 P. Schummer, K. H. Tebel, *J. Non-Newtonian Fluid Mech.* **1983**, *12*, 331–347.

33 E. Greiciunas, J. Wong, I. Gorbatenko, J. Hall, M. Wilson, N. Kapur, O. Harlen, D. Vadillo, P. Threlfall-Holmes, *J. Rheol.* **2017**, *61*, 467–476.

34 D. C. Vadillo, T. R. Tuladhar, A. C. Mulji, S. Jung, S. D. Hoath, M. R. Mackley, *J. Rheol.* **2010**, *54*, 261–282.

35 J. P. Rothstein, *Rheol. Rev.* **2008**, 1–46.

36 R. H. Fernando, L. L. Xing, J. E. Glass, *Prog. Org. Coat.* **2001**, *42*, 283–288.

37 Y. Christanti, L. M. Walker, *Atomization Sprays.* **2006**, *16*, 777–790.

38 B. Keshavarz, V. Sharma, E. C. Houze, M. R. Koerner, J. R. Moore, P. M. Cotts, P. Threlfall-Holmes, G. H. McKinley, *J. Non-Newtonian Fluid Mech.* **2015**, *222*, 171–189.

39 B. Keshavarz, E. C. Houze, J. R. Moore, M. R. Koerner, G. H. McKinley, *Phys. Rev. Lett.* **2016**, *117*, 154502.

40 L. Palangetic, N. K. Reddy, S. Srinivasan, R. E. Cohen, G. H. McKinley, C. Clasen, *Polymer.* **2014**, *55*, 4920–4931.

41 Y. Fang, A. D. Dulaney, J. Gadley, J. M. Maia, C. J. Ellison, *Polymer.* **2015**, *73*, 42–51.

42 S. J. Haward, V. Sharma, C. P. Butts, G. H. McKinley, S. S. Rahatekar, *Biomacromolecules.* **2012**, *13*, 1688–1699.

43 C. J. S. Petrie, Elongational Flows; Pitman: London, **1979**.

44 G. McKay, J. Ferguson, N. Hudson, *J. Non-Newtonian Fluid Mech.* **1978**, *4*, 89–98.

45 C. D. Han, L. Segal, *J. Appl. Polym. Sci.* **1970**, *14*, 2973–2998.

46 F. T. Trouton, *Proc. R. Soc. London A.* **1906**, *77*, 426–440.

47 G. H. McKinley, T. Sridhar, *Annu. Rev. Fluid Mech.* **2002**, *34*, 375–415.

48 M. Stelter, G. Brenn, A. L. Yarin, R. P. Singh, F. Durst, *J. Rheol.* **2000**, *44*, 595–616.

49 M. Stelter, G. Brenn, A. L. Yarin, R. P. Singh, F. Durst, *J. Rheol.* **2002**, *46*, 507–527.

50 F. J. Galindo-Rosales, M. A. Alves, M. S. N. Oliveira, *Microfluidics Nanofluidics.* **2013**, *14*, 1–19.

51 A. Bazilevsky, V. Entov, A. Rozhkov, Third European Rheology Conference and Golden Jubilee Meeting of the British Society of Rheology; Elsevier: Edinburgh, UK, **1990**, pp 41–43.

52 A. V. Bazilevsky, V. M. Entov, A. N. Rozhkov, *Fluid Dyn.* **2011**, *46*, 613–622.

53 R. F. Liang, M. R. Mackley, *J. Non-Newtonian Fluid Mech.* **1994**, *52*, 387–405.

54 V. Tirtaatmadja, G. H. McKinley, J. J. Cooper-White, *Phys. Fluids* **2006**, *18*, 043101.

55 A. Ardekani, V. Sharma, G. H. McKinley, *J. Fluid Mech.* **2010**, *665*, 46–56.

56 A. V. Bazilevskii, V. M. Entov, A. N. Rozhkov, *Polym. Sci. Ser A.* **2001**, *43*, 716–726.

57 E. Miller, C. Clasen, J. P. Rothstein, *Rheol. Acta* **2009**, *48*, 625–639.

58 J. P. Rothstein, *J. Rheol.* **2003**, *47*, 1227–1247.

59 N. J. Kim, C. J. Pipe, K. H. Ahn, S. J. Lee, G. H. McKinley, *Korea-Aust. Rheol. J.* **2010**, *22*, 31–41.

60 M. Chellamuthu, E. M. Arndt, J. P. Rothstein, *Soft Matter.* **2009**, *5*, 2117–2124.

61 A. W. K. Ma, F. Chinesta, T. Tuladhar, M. R. Mackley, *Rheol. Acta* **2008**, *47*, 447–457.

62 D. E. Tsentalovich, A. W. K. Ma, J. A. Lee, N. Behabtu, E. A. Bengio, A. Choi, J. Hao, Y. Luo, R. J. Headrick, M. J. Green, Y. Talmon, M. Pasquali, *Macromolecules.* **2016**, *49*, 681–689.

63 S. L. Anna, G. H. McKinley, *J. Rheol.* **2001**, *45*, 115–138.

64 Y. Amarouchene, D. Bonn, J. Meunier, H. Kellay, *Phys. Rev. Lett.* **2001**, *86*, 3558–3561.

65 V. M. Entov, E. J. Hinch, *J. Non-Newtonian Fluid Mech.* **1997**, *72*, 31–54.

66 R. Prabhakar, S. Gadkari, T. Gopesh, M. J. Shaw, *J. Rheol.* **2016**, *60*, 345–366.

67 R. Prabhakar, C. Sasmal, D. A. Nguyen, T. Sridhar, J. R. Prakash, *Phys. Rev. Fluids* **2017**, *2*, 011301.

68 R. C. Y. Ng, L. G. Leal, *J. Rheol.* **1993**, *37*, 443–468.

69 J. A. Odell, S. P. Carrington, *J. Non-Newtonian Fluid Mech.* **2006**, *137*, 110–120.

70 S. J. Haward, V. Sharma, J. A. Odell, *Soft Matter.* **2011**, *7*, 9908–9921.

71 J. A. Odell, A. Keller, M. J. Miles, *Polymer.* **1985**, *26*, 1219–1226.

72 A. J. Müller, J. A. Odell, A. Keller, *J. Non-Newtonian Fluid Mech.* **1988**, *30*, 99–118.

73 T. Q. Nguyen, H. H. Kausch, Flexible Polymer Chains in Elongational Flow: Theory and Experiment; Springer-Verlag: Berlin, **1999**.

74 P. E. Arratia, C. C. Thomas, J. Diorio, J. P. Gollub, *Phys. Rev. Lett.* **2006**, *96*, 144502.

75 R. J. Poole, M. A. Alves, P. J. Oliveira, *Phys. Rev. Lett.* **2007**, *99*, 164503.

76 J. Soulages, M. S. N. Oliveira, P. C. Sousa, M. A. Alves, G. H. McKinley, *J. Non-Newtonian Fluid Mech.* **2009**, *163*, 9–24.

77 A. Varshney, E. Afik, Y. Kaplan, V. Steinberg, *Soft Matter.* **2016**, *12*, 2186–2191.

78 S. J. Haward, G. H. McKinley, A. Q. Shen, *Sci. Rep.* **2016**, *6*,

79 C. Clasen, J. P. Plog, W. M. Kulicke, M. Owens, C. Macosko, L. E. Scriven, M. Verani, G. H. McKinley, *J. Rheol.* **2006**, *50*, 849–881.

80 D. C. Vadillo, W. Mathues, C. Clasen, *Rheol. Acta* **2012**, *51*, 755–769.

81 C. Clasen, J. Eggers, M. A. Fontelos, J. Li, G. H. McKinley, *J. Fluid Mech.* **2006**, *556*, 283–308.

82 C. Clasen, *Korea-Aust. Rheol. J.* **2010**, *22*, 331–338.

83 O. Arnolds, H. Buggisch, D. Sachsenheimer, N. Willenbacher, *Rheol. Acta* **2010**, *49*, 1207–1217.

84 R. G. Larson, *J. Rheol.* **2005**, *49*, 1–70.

85 M. Doi, S. F. Edwards, The Theory of Polymer Dynamics; Oxford University Press: New York, **1986**.

86 M. Rubinstein, R. H. Colby, Polymer Physics; Oxford University Press: New York, **2003**.

87 B. H. Zimm, *J. Chem. Phys.* **1956**, *24*, 269–278.

88 P. E. Rouse Jr., *J. Chem. Phys.* **1953**, *21*, 1272–1280.

89 P.-G. de Gennes, Scaling Concepts in Polymer Physics; Cornell University Press: Ithaca, **1979**.

90 A. Keller, J. A. Odell, *Colloid Polym. Sci.* **1985**, *263*, 181–201.

91 P. G. de Gennes, *J. Chem. Phys.* **1974**, *60*, 5030–5042.

92 C. M. Schroeder, H. P. Babcock, E. S. G. Shaqfeh, S. Chu, *Science.* **2003**, *301*, 1515–1519.

93 P. Pincus, *Macromolecules.* **1976**, *9*, 386–388.

94 P. Pincus, *Macromolecules.* **1977**, *10*, 210–213.

95 L. E. Rodd, T. P. Scott, J. J. Cooper-White, G. H. McKinley, *Appl. Rheol.* **2005**, *15*, 12–27.

96 L. Campo-Deano, C. Clasen, *J. Non-Newtonian Fluid Mech.* **2010**, *165*, 1688–1699.

97 J. E. Mark, Polymer Data Handbook; Oxford University Press, New York, **2009**.

98 C. A. Schneider, W. S. Rasband, K. W. Eliceiri, *Nat. Methods* **2012**, *9*, 671–675.

99 P. P. Bhat, S. Appathurai, M. T. Harris, O. A. Basaran, *Phys. Fluids.* **2012**, *24*, 083101.

100 R. Suryo, O. A. Basaran, *J. Non-Newtonian Fluid Mech.* **2006**, *138*, 134–160.

101 R. Bird, P. Dotson, N. Johnson, *J. Non-Newtonian Fluid Mech.* **1980**, *7*, 213–235.

102 P. P. Bhat, O. A. Basaran, M. Pasquali, *J. Non-Newtonian Fluid Mech.* **2008**, *150*, 211–225.

103 V. Sharma, A. M. Ardekani, G. H. McKinley, *5th Pacific Rim Conference on Rheology (PRCR-5),* Hokkaido University, Sapporo, Hokkaido, Japan, **2010**.

104 T. Sridhar, D. A. Nguyen, R. Prabhakar, J. R. Prakash, *Phys. Rev. Lett.* **2007**, *98*, 167801.

105 R. K. Gupta, D. A. Nguyen, T. Sridhar, *Phys. Fluids* **2000**, *12*, 1296–1318.

106 K.-W. Hsiao, C. Sasmal, J. Ravi Prakash, C. M. Schroeder, *J. Rheol.* **2017**, *61*, 151–167.

107 P. P. Bhat, S. Appathurai, M. T. Harris, M. Pasquali, G. H. McKinley, O. A. Basaran, *Nat. Phys.* **2010**, *6*, 625–631.

108 M. S. N. Oliveira, G. H. McKinley, *Phys. Fluids* **2005**, *17*, 071704:071701–071704.

109 R. Sattler, S. Gier, J. Eggers, C. Wagner, *Phys. Fluids* **2012**, *24*, 023101.

110 R. Sattler, C. Wagner, J. Eggers, *Phys. Rev. Lett.* **2008**, *100*,

111 V. M. Entov, A. L. Yarin, *Fluid Dyn.* **1984**, *19*, 21–29.

112 D. F. James, T. Sridhar, *J. Rheol.* **1995**, *39*, 713–724.

113 Y. Heo, R. G. Larson, *J. Rheol.* **2005**, *49*, 1117–1128.

114 M. Muthukumar, K. F. Freed, *Macromolecules.* **1978**, *11*, 843–852.

115 Y. Liu, Y. Jun, V. Steinberg, *J. Rheol.* **2009**, *53*, 1069–1085.

116 M. C. Rheinstädter, R. Sattler, W. Häußler, C. Wagner, *Phys. B: Condens. Matter* **2010**, *405*, 3690–3693.

117 A. V. Subbotin, A. N. Semenov, *J. Polym. Sci. Part B: Polym. Phys.* **2016**, *54*, 1066–1073.

118 C. Sasmal, K.-W. Hsiao, C. M. Schroeder, J. Ravi Prakash, *J. Rheol.* **2017**, *61*, 169–186.

119 D. Sachsenheimer, B. Hochstein, N. Willenbacher, *Rheol. Acta* **2014**, *53*, 725–739.

120 D. M. Jones, K. Walters, *Rheol. Acta* **1989**, *28*, 482–498.

121 D. A. Z. Wever, F. Picchioni, A. A. Broekhuis, *Prog. Polym. Sci.* **2011**, *36*, 1558–1628.

122 D. Bonn, Y. Amarouchene, C. Wagner, S. Douady, O. Cadot, *J. Phys.: Condens. Matter.* **2005**, *17*, S1195.

123 C. Wagner, Y. Amarouchene, P. Doyle, D. Bonn, *Europhys. Lett.* **2003**, *64*, 823–829.

124 I. Procaccia, V. S. L'vov, R. Benzi, *Rev. Mod. Phys.* **2008**, *80*, 225.

125 M. D. Graham, *Phys. Fluids* **2003**, *15*, 1702.

126 G. Bhatara, E. S. G. Shaqfeh, B. Khomami, *J. Rheol.* **2005**, *49*, 929–962.

127 M. Pasquali, L. E. Scriven, *J. Non-Newtonian Fluid Mech.* **2002**, *108*, 363–409.